Benchmark for modelization of acoustic transmission loss applied to helicopter trim panels

F. Simon, T. Haase, O. Unruh, G.L. Ghiringhelli, A. Parrinello, R. Vescovini

BENCHMARK FOR MODELIZATION OF ACOUSTIC TRANSMISSION LOSS APPLIED TO HELICOPTER TRIM PANELS

F. Simon[1], T. Haase[2], O. Unruh[2], G. L. Ghiringhelli[3], A. Parrinello[3], R.Vescovini[3]

[1]Onera, Centre de Toulouse, e-mail: frank.simon@onera.fr

[2]DLR, German aerospace center, e-mail: thomas.haase@dlr.de, e-mail: Oliver.Unruh@dlr.de

[3]Dipartimento di Scienze e Tecnologie Aerospaziali – Politecnico di Milano

e-mail: gianluca.ghiringhelli@polimi.it

Abstract

This paper describes the physical, mathematical and numerical approaches applied by laboratories of "Helicopter Garteur Action Group AG20" to vibro-acoustic behavior of helicopter trim-panels. The aim of this numerical activity is to conduct a benchmark study involving different models in order to estimate their framework for using for realistic trim panels. The calculated quantity is the acoustic transmission loss allowing to determine the efficiency of panels to reduce an incident noise. It represents the ratio between incident acoustic power, generally produced by a diffuse acoustic field, and the acoustic power radiated by the panel.

1. INTRODUCTION

Transmission Loss (TL) simulations, based on analytic modelling or Finite and Boundary Element-type techniques, can be achieved to evaluate the effect of the main parameters or to optimize the nature and arrangement of layers, specially for trim panels. Nevertheless, because of the computational time needed for an optimization process, analytical or semi-analytical models are widely used, although suited to an infinite panel size or a finite panel size with simple boundary conditions (simply supported, clamped or free conditions). Accurate modelling of multi-layered trim panels for vibration and acoustic analysis presents many difficulties and challenges, mostly due to their highly heterogeneous anisotropic constitution in the thickness direction and the wide frequency range of interest. Effort in modelling plate problems has been and is still currently devoted to identify which aspects of the 3D mechanical behavior should be accounted for and properly modeled in a 2D mathematical framework, in order to obtain sufficiently simple yet reliable models without unnecessary complexity. This is a basic requirement of industry, where the accuracy of the model should not come at the cost of excessive computational expense, in particular if the model is to be used for iterative design and/or optimization studies. The vast majority of approaches available nowadays are based on reducing the 3D problem to a 2D problem coincident with a chosen reference surface of the plate by introducing in advance *ad-hoc* kinematic assumptions about the behavior of the displacement field along the plate's thickness. A cumbersome analysis based on a high-fidelity fully 3D model could be avoided only if the kinematics of the 2D representation is properly enriched so that the essential 3D nature of the problem is correctly described. The analyst should ideally have the freedom of choosing

the effective 2D model to be used according to the geometric and material properties of the trim panel under study and the frequency range of interest. In so doing, the complexity of the model could be calibrated against a desired or required accuracy for the specific problem at hand, without wasting valuable computational time during the design process.

ONERA has developed several analytic models (integrated into the software PIAMCO) to compute the acoustic TL of infinite or finite sandwich panels, with a thick orthotropic core and orthotropic multi-layered laminates (symmetric or dissymmetric). Models consider elastic materials as, for example, homogeneous materials, composite fibers (kevlar, carbon or fiber glass) with resin, visco-elastic materials, honeycombs or foams, described by their stiffness matrix. They can be applied to simulate structural panels of helicopter fuselage [1], trim panels of cabins [2],[3] and "global" walls [4] by the interaction of a structural panel (e.g. mechanical deck) and a trim panel separated by air gap or porous material (blanket). The first model called "multi-layered model" assumes, firstly, that the panel has an infinite curved or plane surface and, secondly, that the dynamic transverse displacement is constant through the thickness, whatever the frequency range. The displacement field can be written for each layer with membrane, bending and shear terms. So, the continuity of displacements and shear stresses is satisfied at the interface of each layer. Nevertheless, there is no continuity in normal stress and shear stresses are supposed to be independent of the thickness. The potential energy and the kinetic energy are calculated by integrating the different energy densities over a volume defined by the thickness of the panel, one wavelength in the direction of bending waves, and per a unit distance. The Lagrange's equations are then used to obtain the unknown parameters for a given incident acoustic field. The Warburton formulation is used for a finite panel with clamped boundary conditions. The second used model concerns symmetric structures with orthotropic multi-layered laminates and a thick orthotropic core whose transverse dilatation is introduced. The formulation of core displacement is similar to that employed by [5] in the case of a single isotropic laminate on each side of the core. The stiffness terms comply with the hypothesis of plane strain (3D). As concerns the external laminates, the displacement and stress fields follow the approach of the "multi-layered" model.

In the lower frequency range a more detailed knowledge of the TL is desirable, *e.g.*, to evaluate the performance of active control methods. Therefore, the DLR uses a finite element simulation including all material properties and boundary conditions and applies a diffuse sound field which is analytically calculated with a hemisphere approach on the finite element mesh. The simulated surface velocities are post-processed with the radiation resistance matrix in order to calculate the radiated sound power.

The Transfer Matrix Method (TMM) has been exploited by PoliMi to assess the vibro-acoustic behavior of trim-panels. Matrix representation of sound propagation is an efficient and largely used tool for modelling plane acoustic fields in stratified media. The problem is formulated in the frequency domain. The layers are assumed to be laterally infinite, and can be of different natures. Nonetheless, at low frequencies, where the effects of size are important, it is essential to include appropriate corrections, accounting for the finite radiating area. An approach, to the specific problem of airborne TLs, is based on a spatial windowing technique. Analytical expressions for the transfer matrices are only available for elastic solids, thin plates, fluids and poro-elastic media. On the basis of the 3D elasticity theory, the transfer matrix of a general anisotropic layer can also be derived. Description of non-homogeneous media, e.g. honeycomb layers, requires homogeneous representation for such structures. PoliMi also exploits the so-called sublaminate concept. Instead of adopting a global kinematic description for the whole laminate, the thickness of the multi-layered plate is subdivided into an arbitrary number of sublaminates, each one containing one or more adjacent physical plies, and different kinematics refinements can be freely introduced in different thickness subregions. When the laminate is modeled by using one single sublaminate, the classical Equivalent Single-Layer (ESL) and LayerWise (LW) models are easily recovered.

2. NUMERICAL MODELS FOR TRANSMMISSION LOSS PREDICTION

Let us consider a rectangular baffled plate lying on the $1-2$ plane (Figure 1) and separating two semi-infinite media characterized by a speed of sound c_0 and a density ρ_0. A plane wave impinges upon the bottom surface of the flat structure at an incidence angle of θ_I with an orientation with respect to the 1 direction defined by the heading angle φ. Both a reflected wave and a transmitted wave will therefore propagate from the interposed medium.

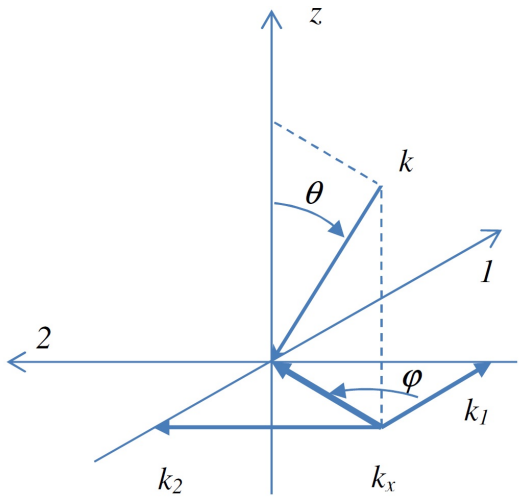

Figure 1: Field and structural system of coordinates

Continuity of the velocity at the bottom interface shows that the angles of incidence and reflection are equal: $\theta_I = \theta_R = \theta$. The angle of transmission, θ_T, and the amplitudes of the reflected and transmitted waves depend on the physical properties of the barrier. With Sommerfeld conditions, the acoustic transmission coefficient can be described by:

$$\tau(\omega, \theta, \varphi) = \frac{P_T}{P_I} \tag{1}$$

where P_I and P_T are the incident and transmitted acoustic powers. In case of a diffuse field excitation, the power transmission factor is defined as

$$\tau_d(\omega) = \frac{\int_0^{2\pi} \int_{\theta_{\min}}^{\theta_{\max}} \tau(\omega, \theta, \varphi) F(\theta) d\theta d\varphi}{2\pi \int_{\theta_{\min}}^{\theta_{\max}} F(\theta) d\theta} \tag{2}$$

where $F(\theta)$ defines the incident field. The most common field used in literature is $F(\theta) = \cos(\theta)\sin(\theta)$ but an isotropic field ($F(\theta) = 1$) fits better with alternative methodologies (see the 286 sources distributed over a hemisphere discussed in Section 2.2) and experimental results reported in the present work. Eventually, the transmission loss is computed as

$$\mathrm{TL}(\omega) = -10 \log(\tau_d(\omega)) \ . \tag{3}$$

2.1 ONERA

In the framework of the "multi-layered model" the displacement field of the i-th layer (Figure 2) can

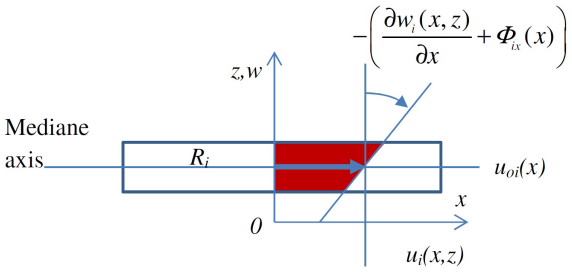

Figure 2: Displacement field in the i-th layer

be defined as:

$$u_i(x,z) = u_{oi}(x) - (z - R_i)\left(\frac{\partial w_i(x,z)}{\partial x} + \varphi_{ix}(x)\right) \tag{4}$$

$$w_i(x,z) = w(x) \tag{5}$$

with u, w displacements in x and z directions, R_i median axis of a layer i, and, respectively, membrane bending and shear terms: $u_{oi}(x)$,$\frac{\partial w_i(x,z)}{\partial x}$,$\phi_{ix}(x)$. As w is assumed to be constant through the thickness, we can define the structural impedance Z_s:

$$Z_s = \frac{p_2 - p_1}{w} \tag{6}$$

and the acoustic coefficient transmission:

$$\tau(\theta, \varphi) = \left(\frac{\omega \rho_0 c_0}{\cos(\theta)}\right)^2 \frac{4}{\left|Z_s - 2\jmath \frac{\omega \rho_0 c_0}{\cos(\theta)}\right|^2} \tag{7}$$

If we consider a finite panel with clamped boundary conditions, the displacement in z direction w can be expressed along (x,y) by:

$$w = \sum_{m=1}^{\infty} \sum_{n=1}^{\infty} \chi_{mn} X_m(x) Y_n(y) \tag{8}$$

with χ_{mn} magnitude of shape $X_m(x)$ $Y_n(y)$ for each mode (m,n) (hypothesis of orthogonality). The displacement field parameters are assumed to be:

$$u_{oi} = \sum_{m=1}^{\infty} \sum_{n=1}^{\infty} \alpha_{imn} X'_m(x) Y_n(y) \tag{9}$$

$$v_{oi} = \sum_{m=1}^{\infty} \sum_{n=1}^{\infty} \beta_{imn} X_m(x) Y'_n(y) \tag{10}$$

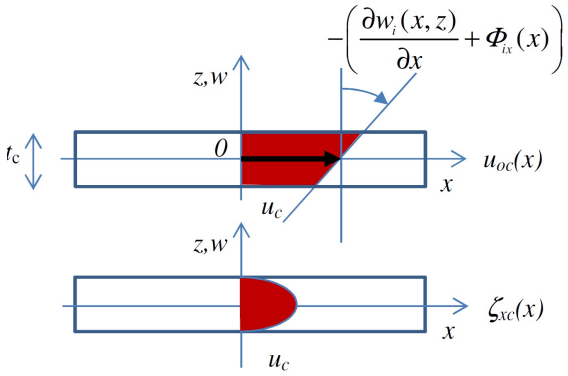

Figure 3: Core displacement in x direction

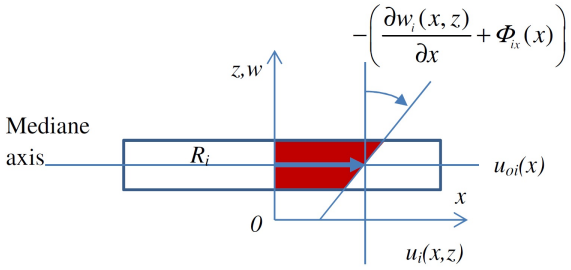

Figure 4: Core displacement in z direction

$$\phi_{ix} = \sum_{m=1}^{\infty}\sum_{n=1}^{\infty} \delta_{imn} X'_m(x) Y_n(y) \tag{11}$$

$$\phi_{iy} = \sum_{m=1}^{\infty}\sum_{n=1}^{\infty} \zeta_{imn} X_m(x) Y'_n(y) \tag{12}$$

For a clamped rectangular panel, $X_m(x)$ $Y_n(y)$ satisfy the Warburton formulation.

For the second used model for which the core is assumed to be thick, the core displacement field satisfies (Figures 3 and 4):

$$u_c(x,z) = u_{oc}(x) + -z\left(\frac{\partial w_c(x,z)}{\partial x} + \varphi_{xc}(x)\right) + \zeta_{xc}(x)\cos\left(\frac{\pi\, z}{t_c}\right) \tag{13}$$

$$w_c(x,z) = \frac{w_{11}(x)+w_{21}(x)}{2} + z\frac{w_{11}(x)-w_{21}(x)}{t_c} \tag{14}$$

with (1,2) the layers 1 and 2 in contact with the core and $x_c(x)$ the expansion term.

It is interesting, for the following, to introduce symmetric (s) and antisymmetric (a) terms to describe relative displacements of external laminates:

$$\begin{aligned} &w_s(x) = \alpha_s \sin(k_x x), w_a(x) = \alpha_a \sin(k_x x), \\ &u_s(x) = \beta_s \cos(k_x x), u_a(x) = \beta_a \cos(k_x x), \\ &\zeta_{xc}(x) = \zeta_{xc} \cos(k_x x) \end{aligned} \tag{15}$$

with

$$\begin{aligned} \alpha_s &= \frac{\alpha_{11}-\alpha_{21}}{2} \quad \text{and} \quad \alpha_a = \frac{\alpha_{11}+\alpha_{21}}{2} \\ \beta_s &= \frac{\beta_{11}+\beta_{21}}{2} \quad \text{and} \quad \beta_a = \frac{\beta_{11}-\beta_{21}}{2} \end{aligned} \tag{16}$$

The transmission coefficient can be described by impedances Z_s and Z_a relative to symmetric and antisymmetric displacements of external laminates:

$$\tau(\theta,\varphi) = \left| \frac{\frac{\rho_0 c_0}{\cos(\theta)}(Z_s - Z_a)}{\left(Z_s + \frac{\rho_0 c_0}{\cos(\theta)}\right)\left(Z_a + \frac{\rho_0 c_0}{\cos(\theta)}\right)} \right|^2 \tag{17}$$

2.2 DLR

The design of active and semi-active methods is relevant for the lower frequency range (up to 1 kHz). Therefore, a detailed finite element simulation of the test-panel was conducted at DLR in the lower frequency range. The frequency band that can be analyzed with finite element methods is limited due to the computational effort which is necessary to increase the frequency range (discretization/number of elements increases with frequency). Six major steps have to be done for a TL simulation:

- generating a diffuse sound field and the pressures on the panel surface
- calculating nodal forces induced by a diffuse sound field
- provide harmonic analysis in the frequency range of interest for the FE-model with applied nodal forces
- export the surface velocities
- post-processing of the velocities with the radiation resistance matrix
- calculation of the TL using incident and radiated sound power.

These major steps are visualized in Figure 5. First of all, the diffuse sound field on the panel surface

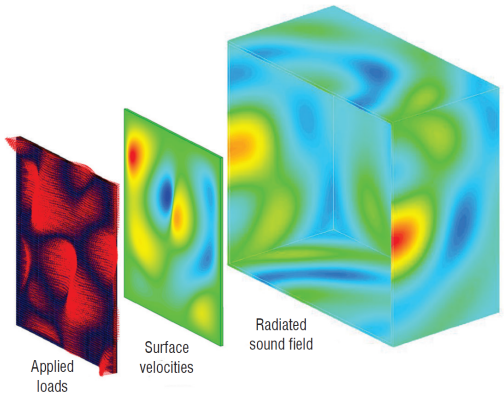

Figure 5: Simulation steps for the TL calculation [8]

has to be generated, which is done with a hemisphere method described in [9]. Therefore, 286 acoustic point sources was distributed over a hemisphere with diameter of 1 meter. The acoustic point sources are driven with the same amplitude but with random phase and the panel is located in a distance of 200m from the hemisphere. After the calculation of the sound pressures on the panel surface they are transferred to nodal forces by using the finite element mesh of the panel. The accuracy of the synthesized diffuse sound field is validated in [10]. The incident sound power due to the diffuse sound field can be calculated by [7]

$$P(\omega) = \frac{S p_{\text{avg}}^2}{4\rho_0 c_0}, \tag{18}$$

where S is the panel area and p_{avg} is the averaged sound pressure of all points on the finite element mesh.
After the calculation of the nodal forces, a harmonic analysis is performed in the FE-software ANSYS and the normal surface velocities are exported for post-processing. An example of the meshing in thickness direction can be seen in Figure 6 for reference panel 2. It has to be noticed that the melamine foam is modeled with volume elements and the other layers with shell elements. The simulation is conducted with 6 elements in thickness direction of the melamine foam. In order to calculate the radiated sound power, the radiation resistance matrix is used [6]. Assuming that the finite element size is small compared to the structural and acoustical wavelength the radiated

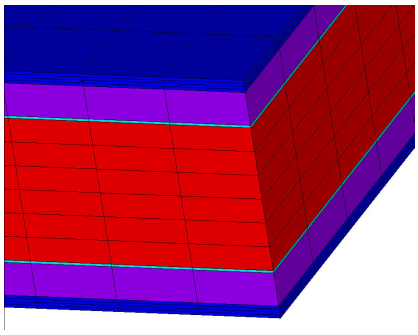

Figure 6: Meshing in thickness direction, glass fabric (blue), honeycomb (purple), glue (cyan) and melamine foam (red)

sound power can be calculated via

$$P(\omega) = \mathbf{v_e}^H(\omega) \cdot \mathbf{R}(\omega) \cdot \mathbf{v_e}(\omega). \tag{19}$$

The normal surface velocities are summarized in the vector $\mathbf{v_e}(\omega)$ and $\mathbf{R}(\omega)$ is the radiation resistance matrix at the circular frequency ω. The radiation resistance matrix is defined by Eq. (20) [6] where S_E is the area of an elemental radiator, k is the wave number and r_{ij} is the distance between the i-th and the j-th elemental radiator.

$$\mathbf{R}(\omega) = \frac{\omega^2 \rho_0 S_E^2}{4\pi c_0} \begin{bmatrix} 1 & \frac{\sin(kr_{12})}{kr_{12}} & \cdots & \frac{\sin(kr_{1N})}{kr_{1N}} \\ \frac{\sin(kr_{21})}{kr_{21}} & 1 & \cdots & \vdots \\ \vdots & \vdots & \ddots & \vdots \\ \frac{\sin(kr_{N1})}{kr_{N1}} & \cdots & \cdots & 1 \end{bmatrix} \tag{20}$$

By using the radiated sound power and the incident sound power the TL can be calculated.

2.3 PoliMi - Transfer Matrix Method

Various types of waves can propagate in each layer of the interposed barrier. The $1-2$ components of the wavenumber of each wave propagating in each layer are equal to the $1-2$ components of the incident wave in the semi-infinite medium, *i.e.*:

$$k_1 = \frac{\omega}{c_0}\sin(\theta)\cos(\varphi)\ , \quad k_2 = \frac{\omega}{c_0}\sin(\theta)\sin(\varphi)\ . \tag{21}$$

The acoustic field in a single layer is completely defined by the nature of the waves propagating in it and by their amplitudes [11].

In a TMM context, each layer of the barrier is replaced by a matrix linking the values of a proper set of variables at the opposite interfaces. First, the

relationship between a set of variables which describe the acoustic field at a specific height, $\mathbf{V}(z_j)$, and the wave amplitudes vector, $\mathbf{A}_j$, must be defined for the j-th layer through a square matrix: $\mathbf{V}(z_j) = \Gamma(z_j)\mathbf{A}_j$. Then, the variables at the bottom interface of the layer, $\mathbf{V}_{Bj}$, can be related to the variables at the top interface, $\mathbf{V}_{Tj}$:

$$\mathbf{V}_{Bj} = \Gamma(z_{Bj})\Gamma(z_{Tj})^{-1}\mathbf{V}_{Tj} = \mathbf{T}_j(\omega,\theta,\varphi)\mathbf{V}_{Tj} \ . \tag{22}$$

The transfer matrix thus obtained for a specific incident plane wave, $\mathbf{T}_j(\omega,\theta,\varphi)$, depends on the thickness and physical properties of the layer. Analytical expressions for the transfer matrices of different kind of layers are available in [11].

The transfer matrix of a layered medium is obtained from the transfer matrices of individual layers by imposing continuity conditions at interfaces as

$$\mathbf{H}_0 = \begin{bmatrix} \mathbf{I}_{f1} & \mathbf{J}_{f1}\mathbf{T}_1 & \cdots & \mathbf{0} \\ \vdots & \vdots & \ddots & \vdots \\ \mathbf{0} & \mathbf{0} & \cdots & \mathbf{0} \\ \mathbf{0} & \mathbf{0} & \cdots & \mathbf{J}_{(n-1)(n)}\mathbf{T}_n \end{bmatrix} \ , \tag{23}$$

where $\mathbf{I}_{ij}$ and $\mathbf{J}_{ij}$ are interface matrices which depend on the nature of the i-th and j-th layers and the suffix f denotes the fluid at the excitation side. Details on the interface matrices are fully available in [11]. For a layered medium with n layers of the same nature interface matrices $\mathbf{I}_{ij}$ and $\mathbf{J}_{ij}$ are identity matrices and the global transfer matrix becomes

$$\mathbf{H}_0 = \begin{bmatrix} \mathbf{I}_{f1} & \mathbf{J}_{f1}\mathbf{T} \end{bmatrix} \ , \tag{24}$$

where

$$\mathbf{T} = \mathbf{T}_1 \cdot \mathbf{T}_2 \cdot ... \cdot \mathbf{T}_n \ . \tag{25}$$

At the termination side, impedance conditions relating the field variables are needed to well pose the problem. Such conditions closely depend on the nature of the termination: hard wall or semi-infinite fluid. The added equations and variables leads to the matrix $\mathbf{H}$ [11].

Enforcing the impedance condition of the fluid at the excitation side allows to calculate the acoustic indicators of the problem. The surface impedance of the medium is calculated by

$$Z_s = -\frac{\det \mathbf{H}_1}{\det \mathbf{H}_2} \ , \tag{26}$$

where $\det \mathbf{H}_i$ is the determinant of the matrix obtained when the i-th column is removed from $\mathbf{H}$. The classical expression for the reflection coefficient is [11]

$$R = \frac{Z_s \cos(\theta) - Z}{Z_s \cos(\theta) + Z} \ , \tag{27}$$

where $Z = \rho_0 c_0$ is the characteristic impedance of the semi-infinite medium. In case of semi-infinite fluid termination, the transmission coefficient, T, and the reflection coefficient, R, are related by

$$\frac{p_1}{1+R} = \frac{p_2}{T} \ , \tag{28}$$

where p_i is the pressure in the i-th semi-infinite fluid, so obtaining the transmission coefficient

$$T = -(1+R)\frac{\det \mathbf{H}_{N+1}}{\det \mathbf{H}_1} \tag{29}$$

and the power transmission factor for the infinite structure:

$$\tau_\infty(\omega,\theta,\varphi) = |T(\omega,\theta,\varphi)|^2 \ . \tag{30}$$

The classical TMM assumes a structure of infinite extent, flat interfaces and homogeneous (and isotropic) layers. The last two limitations can be overcome by involving a FE model for the periodic unit cell of each heterogeneous layer [12]. So, the TMM makes it possible to accurately and efficiently assess the sound transmission through any planar structure with arbitrary stratification and infinite extent. A simple geometrical correction to account for finite size effect is presented. The approach consist on replacing the radiation efficiency in the receiving domain by the radiation efficiency of an equivalent baffled window. This approach is thus strictly valid for planar structures. The power transmission factor accounting for the finite size effect, τ, is related to the classical factor, τ_∞, by [11]

$$\tau = \tau_\infty \sigma_R \cos(\theta) \ . \tag{31}$$

The geometrical radiation efficiency, σ_R, for a rectangular baffled plate with in-plane dimensions $a \times b$ can be expressed as

$$\sigma_R(k_0,\theta,\varphi) = \frac{abk_0}{\pi^2}\int_0^{k_0} \frac{kH}{\sqrt{k_0^2 - k^2}} dk \ , \tag{32}$$

where $k_t = k_0 \sin(\theta)$, $k_0 = \omega/c_0$ and

$$H(k) = \int_0^{2\pi} \frac{1-\cos(ka\cos(\psi) - k_t a\cos(\varphi))}{(ka\cos(\psi) - k_t a\cos(\varphi))^2} \cdot \frac{1-\cos(kb\sin(\psi) - k_t b\sin(\varphi))}{(kb\sin(\psi) - k_t b\sin(\varphi))^2} \cdot d\psi \tag{33}$$

2.4 PoliMi - Sublaminate variable-kinematics Ritz models

A very flexible modelling technique for composite structures capable of generating, within a unified mathematical framework, a virtually infinite number of plate models based on arbitrary-order 2D theories of different typologies is here briefly presented. The present technique comes with a characteristic *variable-kinematic* property, which means that the formulation is invariant with respect to the choice of a specific plate theory.

The fundamental element is the sublaminate, which is defined as a specific group of adjacent material plies with a specific 2D kinematic description, i.e., the theory adopted to approximate the displacement field across the thickness of the sublaminate. Accordingly, each sublaminate is associated with the number of plies of the sublaminate, the first and last ply constituting the sublaminate and the local kinematic description (ESL or LW). The order of the theory can be chosen independently from sublaminate to sublaminate.

The formulation is based on the geometric description illustrated in Figure 7. The multilayered panel of total thickness h is assumed to be composed of N_p physical plies of homogeneous orthotropic material and thickness h_p. For modelling purpose, the laminate is arbitrarily subdivided into $k = 1, 2, \ldots, N_k$ sublaminates of thickness h_k. When $N_k = 1$, $h_k = h$ and a classical single model is retrieved, *i.e.*, one sublaminate coincident with the whole laminate. In general, $N_k \leq N_p$. All the relevant quantities belonging to ply p of sublaminate k are indicated with the superscript $()^{p,k}$. Each sublaminate is associated with a specific kinematic description, both in terms of theory and order of the expansion. The 3D displacement field associated to the generic ply p of the sublaminate k is denoted as $\mathbf{u}^{p,k} = \left\{ \begin{array}{ccc} u_x^{p,k} & u_y^{p,k} & u_z^{p,k} \end{array} \right\}^{\mathrm{T}}$ and each component is postulated in a layerwise manner as follows:

(34)
$$
\begin{aligned}
u_x^{p,k}(x,y,z_p,t) &= F_{\alpha_{u_x}}(z_p) u_{x\alpha_{u_x}}^{p,k}(x,y,t), \ \alpha_{u_x} = 0..N_{u_x}^k \\
u_y^{p,k}(x,y,z_p,t) &= F_{\alpha_{u_y}}(z_p) u_{y\alpha_{u_y}}^{p,k}(x,y,t), \ \alpha_{u_y} = 0..N_{u_y}^k \\
u_z^{p,k}(x,y,z_p,t) &= F_{\alpha_{u_z}}(z_p) u_{z\alpha_{u_z}}^{p,k}(x,y,t), \ \alpha_{u_z} = 0..N_{u_z}^k
\end{aligned}
$$

where z_p is the local ply-specific thickness coordinate, $F_{\alpha_{u_\circ}}(z_p)$ are thickness functions ($\circ = x, y, z$), $u_{\circ\alpha_{u_\circ}}^{p,k}$ is the kinematic variable of the adopted 2D approximation, and $N_{u_\circ}^k$ is the order of expansion. Note that in Eq. (34) the summation is implied for repeated theory's indexes $\alpha_{u_\circ}$ and sublaminate ESL models can be recovered by setting $z_p = z_k$, where z_k is the sublaminate-specific thickness coordinate (see Figure 7). The thickness functions are taken as a proper combination of Legendre polynomials so that the kinematic variables associated to the expansion indexes $\alpha_{u_\circ} = 0, 1$ identify the displacement at the top and the bottom of the ply or sublaminate. This property is particularly useful during the through-the-thickness assembly procedure, as far as the continuity between adjacent plies or sublaminates is easily imposed.

The formulation is developed in the context of a variational displacement-based approach. More specifically, the weak form of the equilibrium equations is expressed by means of the Principle of Virtual Displacements (PVD). Once a specific plate theory is postulated through Eq. (34), the corresponding displacement approximation is substituted into the PVD equilibrium equation so that the original 3-D problem is transformed into a 2-D problem in the $x - y$ plane. The resulting variational form contains 2-D generalized kinematic coordinates, which are further expressed through a Ritz expansion as follows:

(35)
$$
\left\{ \begin{array}{l}
u_{x\alpha_{u_x}}^{p,k}(x,y) = N_{u_x i}(x,y) u_{x\alpha_{u_x} i}^{p,k} \\
u_{y\alpha_{u_y}}^{p,k}(x,y) = N_{u_y i}(x,y) u_{y\alpha_{u_y} i}^{p,k} \quad i = 1..M \\
u_{z\alpha_{u_z}}^{p,k}(x,y) = N_{u_z i}(x,y) u_{z\alpha_{u_z} i}^{p,k}
\end{array} \right.
$$

where $N_{u_\circ 1}, N_{u_\circ 2}, \ldots, N_{u_\circ M}$ is the complete set of global, admissible and linearly independent functions selected to represent each kinematic unknown related to the expansion of the generic displacement component $u_\circ$. In this work, the Ritz set is selected as the product of Chebyshev polynomials and proper boundary functions defined in the computational domain (ξ, η) of the plate, with $\xi \in [-1, 1]$ and $\eta \in [-1, 1]$.

After substituting Eq. (34) and Eq. (35) into the PVD, the discretized weak form of the dynamic equilibrium equations can be expressed in compact form by means of self-repeating building blocks, denoted as fundamental kernels of the formulation, which are invariant with respect to the number of sublaminates, the typology of the local kinematic description (ESL or LW) and the orders of expansion of each local displacement quantity. Accordingly, the proposed approach allows for the hierarchical generation of plate models with different 2-D kinematic descriptions from the same unified mathematical framework. In other words, an appropriate sequence of expansion and assembly procedures of these kernels yields the specific stiffness and mass matrix of the multi-layered plate accord-

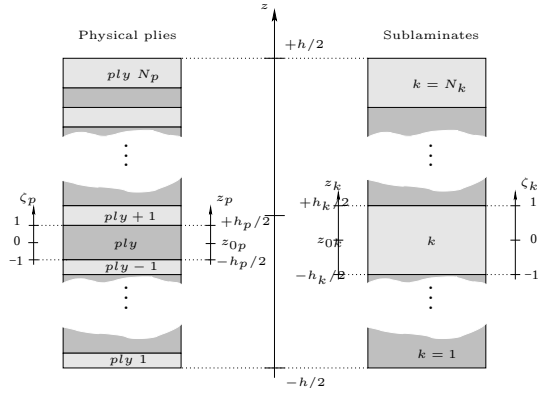

Figure 7: Geometric description.

ing to the selected multiple-kinematic model. If a different model is required, the *same sequence* is repeated starting from the *same building blocks* with the new free parameters of the model (sublaminate subdivision, typology of kinematic description, order of expansion of the displacements, number of terms retained in the Ritz series) to yield the new stiffness and mass matrices of the plate.

The expansion and assembly procedure involves four main steps. The first step deals with the expansion of the kernels according to the summation implied in the repeated indexes α_{u_r} and β_{u_s} $(r, s = x, y, z)$, which arises from the order of the kinematic description postulated in each sublaminate. The second step is the assembly of the ply-contributions in each sublaminate involving a cycling over the index p. All sublaminate contributions are subsequently stacked along the thickness coordinate to account for the continuity of the generic displacement variable at the interfaces between adjacent layers. The sublaminate contributions of different layers are always assembled in a LW manner. The assembly of the sublaminates contributions involves the cycling over the index k. The final step deals with expansion corresponding to the summation implied in the repeated indexes i and j related to the Ritz series approximation of the kinematic quantities. The final set of governing equations takes the following form

$$\mathbf{M\ddot{u}} + \mathbf{Ku} = \mathbf{L}^{\text{top}} f^{\text{top}} + \mathbf{L}^{\text{bot}} f^{\text{bot}} \tag{36}$$

where $\mathbf{u}$ collects all the generalized coordinates of the Ritz expansion corresponding to each variable of the kinematic model assumed in each sublaminate and f^{top} and f^{bot} denote the normal pressure applied at the top and bottom of the panel, respectively.

Fluid loading on the plate is assumed to be small and it is thus neglected. A diffuse field is simulated on one side of the panel by a set of incident plane waves of same amplitude and different incidence angle (θ, φ). With the assumption of a light fluid for the two sides of the plate, the incident pressure field on the top side of the panel can be expressed as

$$f_{\text{top}} = 2e^{-jk\sin\theta(x\cos\varphi + y\sin\varphi)} \tag{37}$$

where $k = \omega/c_0$ is the wavenumber. For each incident wave, the incidence transmission coefficient $\tau(\omega, \theta, \varphi)$ is computed as

$$\tau = \frac{2\rho_0 c_0 P}{S\cos(\theta)} \tag{38}$$

where S is the panel area and the radiated sound power, $P(\omega, \theta, \varphi)$, is evaluated in terms of elementary radiators, Eqs. (19,20). The diffuse transmission loss, TL(ω), is computed according Eqs. (2,3).

3. STUDY CASES

These different models are involved for two types of ONERA "trim" panel used as reference: the first one has a core designed with a nomex honeycomb and the second one with a melamine foam, to produce an added dilatation effect in the frequency range of interest. Only results of "finite" approaches are reported, along with experimental evaluation of TLs. Similarities and differences are analyzed according to particularities of each approach.

3.1 Panel 1

The 1st panel (surface: $0.90 \times 0.90 m^2$) reaches $3.4 kg/m^2$ for a thickness of 11.7 mm (Figure 8). A modal analysis has been conducted with clamped boundary conditions (free surface: $0.84 \times 0.84 m^2$) to verify the mechanical and dimensional characteristics. The computation of resonance frequencies has been led with an analytical vibration model, developed in ONERA, that points out membrane, bending and shear effects with the continuity of displacements and shear stresses at the interface of each orthotropic layer. The theoretical mode shapes follow the Warburton formulation. The simulations are achieved for layers characteristics listed in Table 1. Twenty four modes have been extracted with accuracy between 84 and 1312 Hz with a loss factor between 2 and 20%. The modes shapes are in accordance with the clamped boundary conditions, except for the first modes for which theses conditions are more difficult to achieve.

	Glass fabric	Aramid fabric	Glue	Nomex honey.
ρ (kg/m^3)	1600	1300	1000	32
E_{xx}	16.2	27.5	1.68	(0.001)
E_{yy}	16.2	27.5	1.68	(0.001)
E_{zz}	(1)	(1)	1.68	0.080
G_{yz}	2.75	2.0	0.60	0.013
G_{xz}	2.75	2.0	0.60	0.023
G_{xy}	2.75	2.0	0.60	(0.001)
ν	0.15	0.09	0.4	(0.3)
$\eta(\%)$	1	1	1	3

Table 1: Properties of materials for Panel 1 (elastic moduli are expressed in GPa, values in brackets, required by a full 3D constitutive law, are little relevant with respect to results).

The panel has been tested in the ONERA setup to obtain the experimental acoustic TL with diffused field. The simulation of the TL and the experimental measurement for the panel are compared in Figure 9. It is important to note that, below 200 Hz, assumption of diffused field is not assured experimentally because of ONERA reverberant room characteristics. So, some differences can occur between simulations and experimentation. Globally, experimental tendencies are representative of "mass law". It can be seen that the TL in the frequency range up to 900 Hz is very well approximated. So, simulations follow experimental mean curve with generally a tolerance of $\pm$ 1 dB, except for infinitely extended model (TMM) for which the modal behavior is not taken into account. In this last case, when modal density increases, differences decreases. Even the modal characteristics of the panel (*e.g.* at 480 Hz) are present in the simulation, where the transmission loss curve has major dips compared to analytical models or FE modelization. Above 900 Hz the TL is slightly overestimated, possibly due to the errors in the assumed structural damping in the simulation.

3.2 Panel 2

The 2nd panel (surface: $0.90 \times 0.90m^2$) reaches $4.75kg/m^2$ for a thickness of $21.7mm$ and is composed of "melamine" foam placed between Nomex honeycombs and external fiberglass layers (Figure 10). The manufacturing has been done with the following process:

- Polymerization of "glass fabric / honeycomb" layers under vacuum at 120°C
- Control of total thickness of "glass fabric / honeycomb"
- Application of glue on foam sides with spatula
- "glass fabric / honeycomb" layers + "glue / foam" under vacuum
- Polymerization under mass at 60°C
- Control of total thickness of "glass fabric / honeycomb"

The lay-out is symmetrical to avoid internal stresses generating a panel curvature.

A modal analysis has been conducted with clamped boundary conditions (free surface: $0.84 \times 0.84m^2$) to verify the mechanical and dimensional characteristics. The theoretical mode shapes follow the Warburton formulation. The simulations are achieved for layers characteristics listed in Table 2. Nineteen modes have been extracted by modal analysis, with accuracy, between 23 and 266 Hz with a viscous damping between 2 and 7.5%. The mode shapes are in accordance with the clamped boundary conditions, except for the first modes for which theses conditions are more difficult to achieve.

The simulation of the TL and the experimental measurement for the panel are compared in Figure 11. The high TL is assured thanks to a dilatation effect of foam from medium frequencies and the static bending stiffness thanks to honeycombs. It appears the particular behavior of double wall resonance around 700-800 Hz, frequency band for which the TL increased highly to reach about 60 dB. The simulations led with the previous characteristics (Table 2) follow the tendencies of the experimental TL with, nevertheless a frequency shift that depends on the transverse Young modulus of the foam. The frequency range up to 1200 Hz is very well approximated. Modal behavior is less perceived than for Panel 1 because of presence of double wall resonance that amplifies transverse dilatation.

4. CONCLUSIONS

Because of many constraints the design of an effective trim panels for helicopters is a very challenging task. Numerical methods, independently conceived by the research groups cooperating in Garteur AG20 in the frame of the structural dynamics and applied to vibroacoustics, have been compared. They refer to different implementation of the dynamic structural modelization of a

	Glass fabric	Melamine foam	Glue	Nomex honey.
ρ (kg/m^3)	1600	11.7	1050	96
E_{xx}	21000	0.24	1950	1
E_{yy}	21000	0.24	1950	1
E_{zz}	21000	0.24	1950	330
G_{yz}	3000	0.12	700	85
G_{xz}	3000	0.12	700	38
G_{xy}	3000	0.12	700	1
ν	0.13	0	0.4	0
$\eta(\%)$	1	10	1	5

Table 2: Properties of materials for Panel 2 (elastic moduli are expressed in MPa).

panel under external acoustic loads. Three methods take into account of the finite size of panel, *i.e.* "multi-layered model" (ONERA), FE-model (DLR) and SL Ritz (PoliMI). Two other methods lie in more analytical frames applied to infinite panel *i.e.* "transverse dilatation model" (ONERA) and TMM (PoliMI). In particular, for TMM, exploiting the Transfer Matrix approach, a windowing technique is also required.

The results are satisfactorily comparable despite the difficulties in modelling dynamic problems in the specific frequency range. All the methods are able to catch typical physical phenomena, *e.g.* the TL decay due to the double wall effect in Panel 2. Furthermore they well match with experimental data. In this case the quality of the comparison can be affected by the weighting function chosen in Eq. (2) to represent actual conditions obtained in the reverberant room. All the methods exploit 3D constitutive material relationship, thus some of needed data are often not available from standard testing activities. They can have non negligible effects on the results. The comparison with experiment data testifies the effectiveness of the different approaches that can be used in the frame of actual design.

The little time required by the analysis of "infinite" approaches, few seconds against many minutes of other approaches, and a negligible time for model building make TMM and "transverse dilatation model" suitable candidates for optimization activities.

References

[1] F. Simon, Sound Transmission Loss model of curved multilayered panels, Thirteen International Congress on Sound and Vibration (ICSV13), 8 p., Vienna, July 2006.

[2] F. Simon, S. Pauzin, D. Biron, Modelization and test of composite trim panels for reducing helicopter internal noise, ICSV9 - 9th International Congress on Sound and Vibration, pp. 1-8, Orlando, USA, July 2002.

[3] P. Leite, M. Thomas, F. Simon, Y. Brchet, Optimal Design of a Multifunctional Sandwich Panel With Foam Core: Lightweight Design for Flexural Stiffness and Acoustical Transmission Loss, Advanced Engineering Materials Vol. 17, No 3, pp. 311-318

[4] F. Simon, S. Pauzin, D. Biron, "optimization of sandwich trim panels for reducing helicopter internal noise, ERF30, Marseille, France, September 2004.

[5] Moore and Lyon, Sound transmission loss characteristics of sandwich panel constructions Journal of the Acoustical Society of America 89(2), Feb. 1991

[6] Fahy, Frank J and Gardonio, Paolo, Sound and structural vibration: radiation, transmission and response, Academic press, 2007.

[7] Möser, Michael, Technische Akustik, Springer, 2005, Vol.8.

[8] Simon, Frank and Haase, Thomas and Unruh, Oliver and Pohl, Martin and Tijs, Emiel and Wijntjes, Rik and Van Der Wal, H and Ghiringhelli, GL, Activities of european research laboratories regarding helicopter internal noise., AerospaceLab, 2014, 7, pp. p-1.

[9] Witting, Michael, Modelling of diffuse sound field excitations and dynamic response analysis of leightweight structures, Herbert Utz Verlag, 1999.

[10] M. Misol, C. Bloch, H. P. Monner, M. Sinapius; Performance of active feedforward control systems in non-ideal, synthesized diffuse sound fields. The Journal of the Acoustical Society of America 135 (2014) 1887-1897.

[11] Allard, J. F., Atalla, N.: Propagation of sound in porous media: Modelling sound absorbing materials - Second edition. John Wiley and Sons, Ltd, Chichester, 2009.

[12] A. Parrinello, G. Ghiringhelli: Transfer matrix representation for periodic planar media. Journal of Sound and Vibration 371 (2016) 196-209.

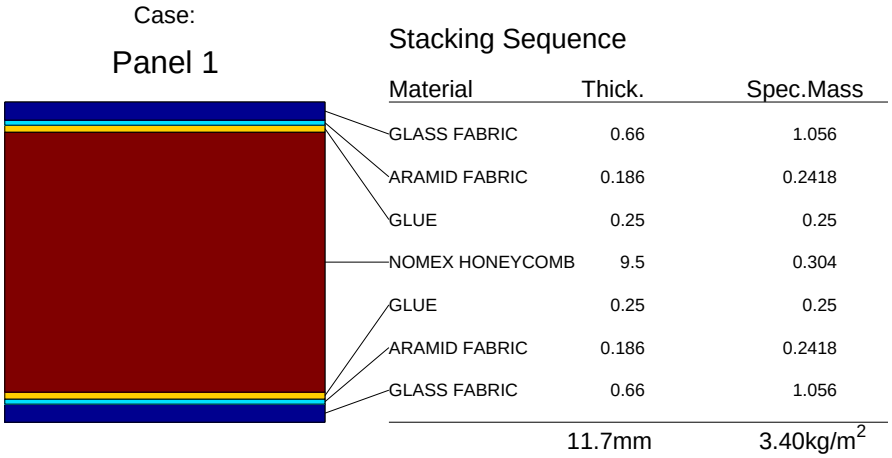

Figure 8: Panel 1

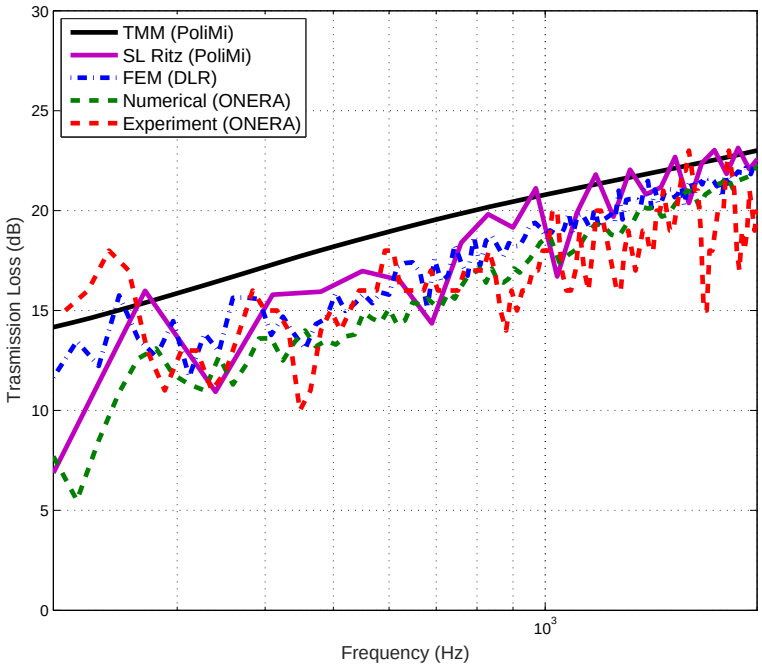

Figure 9: TL simulations and measurement for Panel 1

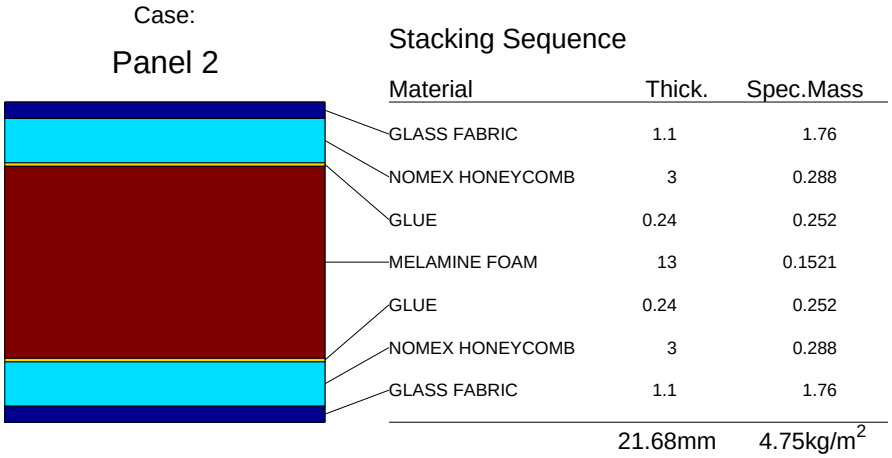

Figure 10: Panel 2

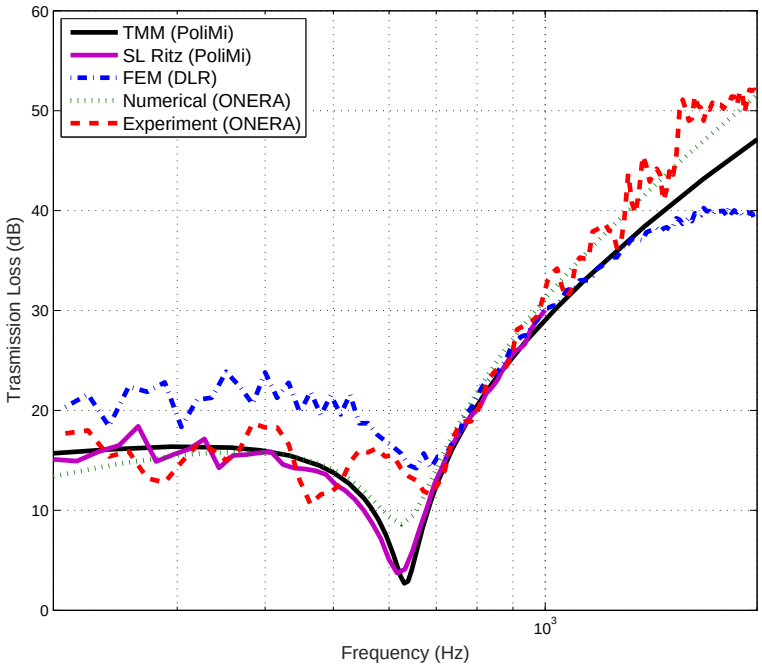

Figure 11: TL simulations and measurement for Panel 2